A spectroscopic and computational study of a tough MOF with a fragile linker: Ce-UiO-66-ADC.

A spectroscopic and computational study of a tough MOF with a fragile linker: Ce-UiO-66-ADC

Alessia Airi [a], Cesare Atzori[a*], Francesca Bonino[a], Alessandro Damin[a], Sigurd Øien-Ødegaard[b], Erlend Aunan[b] and Silvia Bordiga[a,b *]

The thermolabile acetylene dicarboxylic acid has been introduced as linker in UiO-66 topology, synthetizing the compound with formula $[Ce_6O_4(OH)_4(ADC)_6]$ and denoted as Ce-UiO-66-ADC MOF. The characterization by multi-technique approach coupled with computational modelling revealed a peculiar intrinsic defective nature related to the nature of the linker.

Metal-organic frameworks (MOFs) represent a rather new class of synthetic crystalline materials, constituted by discrete inorganic (metal-oxide clusters) and organic (multitopic organic linkers) units, connected together by coordination bonds.[1,2] The units represent the building blocks for the formation, through their opportune choice and combination,[3] of a large variety of different structures, in which the metal-oxide clusters occupy the nodes and are connected to each other by the ligands, which act as spacers, originating an ideal porous system.[4–7] Thanks to the possibility to predict and to tailor their lattices and composition, over the last two decades, MOFs have been the object of increasing interest. Moreover, these materials may be characterized by high specific surface areas, tuneable pore size and chemical functionalities, opening a wide landscape on potential applications in various fields, among which catalysis[8,9] and gas adsorption and storage are emerging.[10,11]

Since its discovery in 2008,[12] the MOF denoted as UiO-66 $[Zr_6O_4(OH)_4(BDC)_6]$, has attracted considerable attention by the scientific community, mainly because of its exceptional toughness: it resists at temperature around 400°C, it shows considerable resistance to hydrolysis and also high tolerance for defects.[13] Moreover, the formation of the cubic lattice by self-assembling of the Zr(IV) clusters (in presence of linear dicarboxylic linkers) is so favoured that the formation of secondary phases, in the same synthetic conditions, is avoided;[14] this encouraged the fruitful research of UiO-66 isostructural derivatives obtained by changing the linker or the metal cation.[15–18] In this scenario, the present work aimed to introduce the acetylene dicarboxylate (ADC), as linker in the UiO-66 framework and full characterize its peculiar features. The thermal lability and quite reactive nature of the precursor molecule (the acetylene dicarboxylic acid H_2ADC undergoes very easily to decarboxylation), made it an almost forgotten linker in the history of MOFs,[19,20] even if a consistent literature on ADC-based coordination polymers is known.[21–29] On the other hand, recently, it was demonstrated that it is possible to obtain the structure of UiO-66, using Cerium(IV) as metal centre.[30] It was attested that Ce(IV) admits the same coordination of Zr(IV) and the same topology of the MOF, while it offers much shorter times and milder conditions for the synthesis, opening a new fruitful research concerning Ce-UiO-66 derivatives[31–36]and for the introduction of ADC.[37]

With the aim to observe the behaviour of the thermolabile molecule within the UiO-66 lattice, we synthetized the MOF hereafter called Ce-UiO-66-ADC, which contains Ce(IV) as metal cation and ADC as organic linker, following the sub-solvothermal method developed for Ce(IV) UiO-66 derivatives by Lammert et al. in 2015.[30]

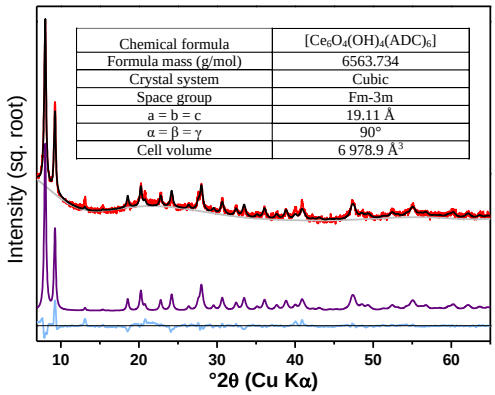

Figure 1. Rietveld refinement of PXRD pattern of Ce-UiO-66-ADC (black). The Rietveld fitted curve is shown in black, the deconvoluted pattern in violet, the background in grey and the residuals in blue. The position of Ce atoms was allowed to refine freely, whereas the other atoms (O, C) were fixed to force field-optimized positions. Inset: table containing the most relevant structural details.

More in detail, the acetylene dicarboxylic acid (H_2ADC) was solubilized in dimethylformamide (DMF), then a 0.53M aqueous solution of $[(NH_4)_2[Ce(NO_3)_6]$ (CAN) was added to the first one. The quantities were calculated to obtain a 1:1 molar ratio between the metal precursor and the organic linker. The closed vial was then inserted in oven at 90°C for 15 minutes (see ESI, section 1.1). The procedure described above produced a yellowish powder with a yield of about 5%. Powder X-Ray diffraction (PXRD) proved that the product is composed by a single crystalline phase showing the principal reflexes of UiO-66 pattern, thus confirming the success of the synthesis. On the other hand, the transmission IR spectroscopy (see ESI, Figure S1), performed on outgassed sample, revealed intense signals of an unexpected species. The bands at 3260 cm^{-1} (m) due to ν

[a] *Department of Chemistry, NIS and INSTM Reference Centre, University of Torino, Via G. Quarello 15, 10135 Torino, Italy*
[b] *Catalysis Section, Department of Chemistry, University of Oslo, P.O. Box 1033, N-0315 Oslo, Norway*

C≡(**C-H**) and at 2107 cm^{-1} (s) due to ν R-(**C≡C**)-H, are compatible with the presence of a terminal alkyne.[38] This first analysis suggested that the linker undergoes a decarboxylation reaction caused by the heating, justifying a so low yield. In fact, a systematic study concerning decarboxylation of H_2ADC, conducted by Li et al. in 2002,[39] reports that the presence of H_2O favours the decarboxylation and allows it to occur at lower temperatures (already at 60°C). Water accelerates the process stabilizing a transition state in which it mediates the transfer of acid protons from the carboxylic acid to the α-carbon, forming a stable terminal alkyne. H_2ADC and $HADC^-$, possesses acid protons thus they can easily undergo the water mediated decarboxylation at the synthetic temperature (90°C-100°C). The reaction products are the terminal alkynes, propiolic acid and propiolate anion (Scheme 1). On the basis of this hypothesis, the reason of a so low yield, is ascribable to a loss of the pristine linker that, if reacted, is not available anymore to build the framework.

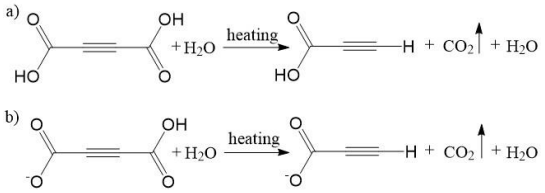

Scheme 1. a) Water mediated decarboxylation of ADC, producing propiolic acid. b) Water mediated decarboxylation of ADC^-, producing propiolate anion.

The decarboxylation reaction is, in fact, in competition with the reaction of self-assembling that induces the linker to react with the metal ion, to give rise to the three-dimensional structure of the MOF. For this reason, the synthesis was improved introducing a Brønsted base (triethylamine) in the reaction mixture in ratio 1:1 respect to the reagents, in order to stabilize the double deprotonated form (ADC^{2-}) that is much less converted into propiolate. Therefore, in basic solution a higher amount of linker would be preserved from decarboxylation and would be available to interact directly with Cerium to form the MOF lattice. The synthesis in basic conditions was performed following the same procedure already described, after mixing reactants, the solution was treated in oven at 100°C for 15 minutes (see ESI, section 1.1a). This strategy resulted to be successful: the expected crystal phase was obtained as evidenced by PXRD (see ESI, Figure S2) and the yield raised to about 40%. Obtaining a relevant amount of sample, a deep multitechnique characterization was performed, first collecting information about the bulk structure and its stability, then studying the finest features by means of vibrational spectroscopies and computational modelling. The morphology of the MOF crystals has been explored by SEM and TEM microscopy, showing spherical particles that do not exceed the nanometric size (ESI, Figures S3-4). The crystal structure was refined by Rietveld method, using the UiO-66 lattice as starting guess (space group Fm-3m) for refining the diffractogram of the sample obtained by Micro Wave irradiation (following the aforementioned synthetic strategy, see ESI Section 1.1b, for further details), considerable as reference compound, because of the better quality of the pattern. Figure 1 shows the isostructurality with UiO-66, indicating an FCC packed structure with stoichiometry $Ce_6O_4(OH)_4(ADC)_6$ (the structural details are reported in ESI in section 3.4 and Figure S5). In order to obtain a first clue concerning the main electronic and vibrational features of the ideal material, the refined structure has been the subject of periodic DFT(B3LYP) based calculations (see ESI section 4 and table S1, for further details) by exploiting the whole capabilities offered by the CRYSTAL17 code. The fully optimized cell (F-43m) resulted to have a = 19.18 Å and V = 7058.4 $Å^3$. No negative frequencies are obtained on such structure, confirming its relative stability. As far as the electronic features are concerned, a Eg = 3.04 eV is obtained (see ESI, Figure S6 for density of States). The DRS-UV-Vis spectrum of the Ce-UiO-66-ADC (see ESI, Figure S7) is characterized by an edge at around 400 nm, that finds a correspondence in the computed band gap. The close inspection of the computed DOSs shows that the major contributions to the highest occupied states below the Fermi level (E_0), become from Oxygen and Carbon atoms of the linker, with a minor contribution due to cluster Oxygen atoms; while the lower unoccupied state above E_0 corresponds to Cerium orbitals. This suggests that the lowest observed energy absorption corresponds to a ligand to metal charge transfer (LMCT) that explain the yellow colour of the material. Studies concerning thermal stability started with variable temperature X-Ray diffraction (VTXRD), showing that the diffraction pattern remains almost unvaried until 90°C, marking the thermal limit for crystal structure (see ESI, Figure S8). Over 90°C the crystallinity loss is visible from a gradual disappearance of the principal reflex, positioned at 2θ = 7.9°. At the same time, the TGA curves (see ESI, Figure S9) show a rapid weight loss, starting below 100°C with a first onset point around 150°C, while the DMF loss in indistinguishable. The latter is an important information if combined with VTXRD results. It is clear that the crystalline structure collapses before the degradation occurs (weight loss in TGA), suggesting that, as long as the MOF shows a crystalline structure (until 90°C), the solvent is still trapped into the cavities. Also reasonably, DMF has a role in stabilizing the porous system, as confirmed by 77K N_2 adsorption results, collected in order to point out the specific surface area and the porosity of the MOF. Adsorption measurements were carried out on sample aliquots previously thermally outgassed in vacuum at rising temperature (RT, 60°C, 90°C, 120°C). The obtained isotherms are describable as Type I (see ESI, Figure S10) indicating a microporous system. The surface area has been calculated by B.E.T. (taking in account the Rouquerol rules)[40] and Langmuir models, obtaining the values reported in ESI, Table S2. The material reveals an accessible surface area that can be related to the microporous system, since it grows by increasing the temperature from RT to 60°C (partial removal of the trapped solvent) and it decreases with the collapse of the structure (over 90°C). The very mild outgassing temperature

allows to obtain a considerable value of Langmuir surface area of about 400 m^2/g, but it corresponds to 1/3 of the calculated one (1131 m^2/g see ESI, Section7), because the temperature is too low to completely remove the DMF from the pores. In situ FT-IR and Raman measurements were collected along thermal activation under high vacuum, from RT (black curves) to 90 °C (violet curves), as shown in Figure 2. In the high frequency region (3800-2800 cm^{-1}), the infrared spectrum is dominated by intense broad bands that goes out of scale due to presence of the adsorbates interacting by H-bonds (water and DMF). A prolonged in vacuum activation allows to reveal other signals ascribable[38] to both the MOF and the adsorbed solvent (90°C is not enough to completely remove DMF): 3620 cm^{-1} (w) ν(O-H); 3260 cm^{-1} (m) ν(C-H) of terminal alkyne; 2935 cm^{-1} (m) 2810 cm^{-1} (w) respectively $\nu(C\text{-}H)_{sym}$ and $\nu(C\text{-}H)_{asym}$ stretching of N,N amide aliphatic groups; 2107 cm^{-1} (s) ν(C≡C) of asymmetrically substituted alkyne; 1690-1280 cm^{-1} $\nu(COO^-)$ saturated zone containing symmetric and asymmetric modes of framework carboxylate groups (region omitted in Figure 2). Signals related to amides (N-aliphatic CH of methyl groups) indicate the unequivocally presence of reaction solvent (DMF). The bands at 3260 and 2107 cm^{-1} (marked with asterisks in Figure 2) are very informative, indicating also in this case, the presence of propiolates produced by ligand decarboxylation during synthesis. Meanwhile the presence of acetylene dicarboxylate was ascertained by a parallel experiment performed by micro-Raman using an incident laser of 785 nm. The results are illustrated in the inset of Figure 2. In this case, it is observed the appearance of two components at 2235 cm^{-1} and at 2107 cm^{-1}, due to ν (R-**C≡C**-R) and ν (R-**C≡C**-H), respectively gate and asterisk in Figure 3. The assignments of the two bands are confirmed by the comparison of the Raman spectrum of the MOF with those collected on two reference compounds: acetylene dicarboxylate (dark green) and propiolate (light green) in basic aqueous solutions (Figure 3). The first band is ascribable to the MOF linker ADC (symmetric alkyne), while the second one to the propiolate (terminal alkyne). Note that signals related to propiolate do not change in intensity during heating (Figure 2), suggesting that such species is most probably connected to the framework and its incorporation is independent to the synthetic procedure, so it is considerable as a feature of the material. As the monocarboxylic propiolate can chelate only on one side the cluster, while the terminal alkyne remains free, the expected material would be characterized by point defects. It is compatible with the very high tolerance for defectivity reported for UiO-66 structure by many different experimental and computational studies, that opened the way for systematic studies about defect engineering of this kind of MOFs, expanding their properties and functionalities.[41–43] As introduced before, Ce-UiO-66-ADC is characterized by a strong absorption around 400 nm associated to a LMCT transition (Figure S6). This opens the possibility to observe the enhancement of some bands by means of the Raman Resonance effect when the sample is probed by an exciting laser line of the correct wavelength. Figure 4 shows the Raman spectra of Ce-UiO-66-ADC collected with three lasers having different wavelengths (785 nm, 514 nm and 442 nm).

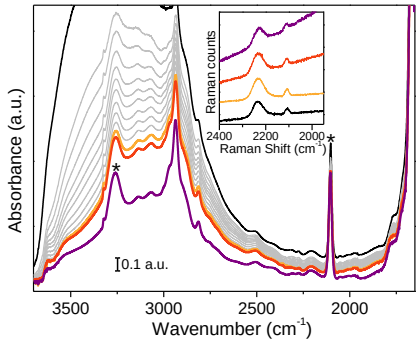

Figure 2. FT-IR spectra collected during Ce-UiO-66-ADC thermal activation. Inset: Raman spectra reported in the 2400-1900 cm^{-1} (triple bonds stretching region) range collected with λ_{inc} = 785 nm. Black: as synthetized RT; grey: in vacuum RT outgassing; yellow: 30°C; orange: 60°C; violet: 90°C.

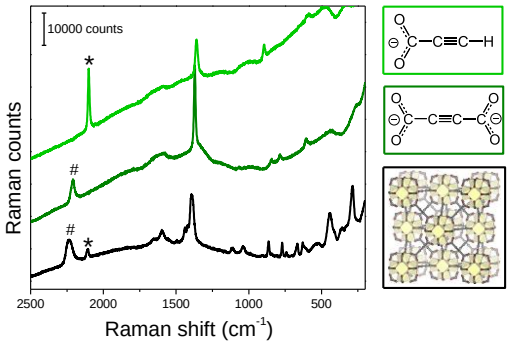

Figure 3. Raman spectra (λ_{inc} = 785 nm) of: Ce-UiO-66-ADC (black), acetylene dicarboxylate solution (dark green), propiolate solution (light green).

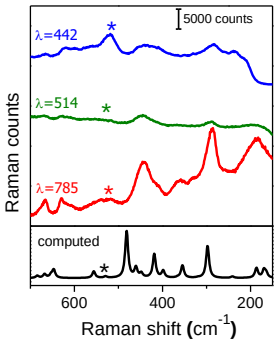

Figure 4. Ce-O cluster vibrational modes region of Raman spectra of Ce-UiO-66-ADC acquired with different λ_{inc}. Black line: computed spectrum.

The most relevant observation is that λ_{inc} = 442 nm causes an increase in relative intensity of the band observed at 521 cm^{-1}. The analogous band in the simulated spectrum is found, as expected, at higher frequencies (556 cm^{-1}) and is due to a complex vibrational mode of the cluster where the major contribution is given by the Ce-O bond stretching of the cluster. The complete assignation is reported in ESI as comparison between experimental and computed frequencies of the principal vibrational modes (see ESI, Table S3).

In conclusion, it has been demonstrated the possibility to obtain an UiO-66 derivative containing the acetylene dicarboxylate as linker, in presence of Ce(IV) as metal centre. This work

highlighted that the reactive and extremely thermolabile nature of the linker implies the necessity of protecting it from decarboxylation reaction in aqueous medium, by Brønsted base addition, which is then removed by washing. This strategy allows to improve the yield from about 5% to about 40%. The combined use of vibrational spectroscopies and DFT calculations revealed an intrinsic defective structure of the material: the product of linker decarboxylation takes part in the framework, implying the loss of connectivity with metal centres, and constituting a local defect. The presence of the terminal alkyne can be used profitably in further studies, as it could represent an expansion of specific surface area; in addition, the functional group could be used as an anchor point for the functionalization of the MOF. For this reason, it is strictly necessary an effective removal of the solvent and the study is already underway.

1 S. Kaskel, *The Chemistry of Metal-Organic Frameworks: Synthesis, Characterization, and Applications*, Wiley-VCH Verlag GmbH & Co. KGaA, Weinheim, Germany, 2016.

2 J. L. C. Rowsell and O. M. Yaghi, *Microporous Mesoporous Mater.*, 2004, **73**, 3–14.

3 N. Stock and S. Biswas, *Chem. Rev.*, 2012, **112**, 933–969.

4 O. M. Yaghi, M. O'Keeffe and M. Kanatzidis, *J. Solid State Chem.*, 2000, **152**, 1–2.

5 J. Kim, B. Chen, T. M. Reineke, H. Li, M. Eddaoudi, D. B. Moler, M. O'Keeffe and O. M. Yaghi, *J. Am. Chem. Soc.*, 2001, **123**, 8239–8247.

6 O. M. Yaghi, M. O'Keeffe, N. W. Ockwig, H. K. Chae, M. Eddaoudi and J. Kim, *Nature*, 2003, **423**, 705–714.

7 M. Eddaoudi, D. B. Moler, H. Li, B. Chen, T. M. Reineke, M. O'Keeffe and O. M. Yaghi, *Acc. Chem. Res.*, 2001, **34**, 319–330.

8 A. Corma, H. García and F. X. Llabrés i Xamena, *Chem. Rev.*, 2010, **110**, 4606–4655.

9 J. Gascon, A. Corma, F. Kapteijn and F. X. Llabrés i Xamena, *ACS Catal.*, 2014, **4**, 361–378.

10 K. Sumida, D. L. Rogow, J. A. Mason, T. M. McDonald, E. D. Bloch, Z. R. Herm, T.-H. Bae and J. R. Long, *Chem. Rev.*, 2012, **112**, 724–781.

11 J. Yang, Q. Zhao, H. Xu, L. Li, J. Dong and J. Li, *J. Chem. Eng. Data*, 2012, **57**, 3701–3709.

12 J. H. Cavka, S. Jakobsen, U. Olsbye, N. Guillou, C. Lamberti, S. Bordiga and K. P. Lillerud, 2008, **6**, 13850–13851.

13 L. Valenzano, B. Civalleri, S. Chavan, S. Bordiga, M. H. Nilsen, S. Jakobsen, K. P. Lillerud and C. Lamberti, *Chem. Mater.*, 2011, **23**, 1700–1718.

14 S. Øien-Ødegaard, G. C. Shearer, K. P. Lillerud and S. Bordiga, in *Nanosponges*, ed. Francesco Trotta Andrea Mele, Wiley-VCH Verlag GmbH & Co. KGaA, Weinheim, Germany, First., 2019, pp. 59–121.

15 D. Zhao, D. J. Timmons, D. Yuan and H.-C. Zhou, *Acc. Chem. Res.*, 2011, **44**, 123–133.

16 S. J. Garibay and S. M. Cohen, *Chem. Commun.*, 2010, **46**, 7700.

17 V. Bon, I. Senkovska, M. S. Weiss and S. Kaskel, *CrystEngComm*, 2013, **15**, 9572.

18 M. J. Katz, Z. J. Brown, Y. J. Colón, P. W. Siu, K. A. Scheidt, R. Q. Snurr, J. T. Hupp and O. K. Farha, *Chem. Commun.*, 2013, **49**, 9449.

19 D. J. Tranchemontagne, J. R. Hunt and O. M. Yaghi, *Tetrahedron*, 2008, **64**, 8553–8557.

20 C. Serre, J. Marrot and G. Férey, *Inorg. Chem.*, 2005, **44**, 654–657.

21 C. Robl and S. Hentschel, *Zeitschrift f*r Anorg. und Allg. Chemie*, 1990, **591**, 188–194.

22 C. Robl and S. Hentschel, *Zeitschrift f*r Anorg. und Allg. Chemie*, 1991, **596**, 149–155.

23 A. Michaelides and S. Skoulika, *Cryst. Growth Des.*, 2005, **5**, 529–533.

24 I. Stein and U. Ruschewitz, *Zeitschrift für Anorg. und Allg. Chemie*, 2010, **636**, 400–404.

25 A. Schuy, I. Stein and U. Ruschewitz, *Zeitschrift für Anorg. und Allg. Chemie*, 2010, **636**, 1026–1031.

26 S. Khullar and S. K. Mandal, *RSC Adv.*, 2014, **4**, 39204–39213.

27 D. Hermann, C. Näther and U. Ruschewitz, *Solid State Sci.*, 2011, **13**, 1096–1101.

28 S. Busch, I. Stein and U. Ruschewitz, *Zeitschrift fur Anorg. und Allg. Chemie*, 2012, **638**, 2098–2101.

29 V. K. Gramm, A. Schuy, M. Suta, C. Wickleder, C. Sternemann and U. Ruschewitz, *Zeitschrift fur Anorg. und Allg. Chemie*, 2018, **644**, 127–135.

30 M. Lammert, M. T. Wharmby, S. Smolders, B. Bueken, A. Lieb, K. A. Lomachenko, D. De Vos and N. Stock, *Chem. Commun.*, 2015, **51**, 12578–12581.

31 M. Lammert, C. Glißmann and N. Stock, *Dalt. Trans.*, 2017, **46**, 2425–2429.

32 R. Dalapati, B. Sakthivel, A. Dhakshinamoorthy, A. Buragohain, A. Bhunia, C. Janiak and S. Biswas, *CrystEngComm*, 2016, **18**, 7855–7864.

33 S. Smolders, K. A. Lomachenko, B. Bueken, A. Struyf, A. L. Bugaev, C. Atzori, N. Stock, C. Lamberti, M. B. J. Roeffaers and D. E. De Vos, *ChemPhysChem*, 2018, **19**, 373–378.

34 S. Smolders, A. Struyf, H. Reinsch, B. Bueken, T. Rhauderwiek, L. Mintrop, P. Kurz, N. Stock and D. E. De Vos, *Chem. Commun.*, 2018, **54**, 876–879.

35 X.-P. Wu, L. Gagliardi and D. G. Truhlar, *J. Am. Chem. Soc.*, 2018, **140**, 7904–7912.

36 T. Islamoglu, D. Ray, P. Li, M. B. Majewski, I. Akpinar, X. Zhang, C. J. Cramer, L. Gagliardi and O. K. Farha, *Inorg. Chem.*, 2018, **57**, 13246–13251.

37 T. J. Matemb Ma Ntep, H. Reinsch, J. Liang and C. Janiak, *Dalt. Trans.*, , DOI:10.1039/C9DT03518D.

38 N. B. Colthup, L. H. Daly and S. E. Wiberley, *Introduction to Infrared and Raman Spectroscopy*, Academic Press, 2nd Edition., 1975.

39 J. Li and T. B. Brill, *J. Phys. Chem. A*, 2002, **106**, 9491–9498.

40 M. Thommes, K. Kaneko, A. V. Neimark, J. P. Olivier, F. Rodriguez-Reinoso, J. Rouquerol and K. S. W. Sing, *Pure Appl. Chem.*, 2015, **87**, 1051–1069.

41 C. Atzori, G. C. Shearer, L. Maschio, B. Civalleri, F. Bonino, C. Lamberti, S. Svelle, K. P. Lillerud and S. Bordiga, *J. Phys.*

Chem. C, 2017, **121**, 9312–9324.
42 G. C. Shearer, S. Chavan, J. Ethiraj, J. G. Vitillo, S. Svelle, U. Olsbye, C. Lamberti, S. Bordiga and K. P. Lillerud, *Chem. Mater.*, 2014, **26**, 4068–4071.
43 G. C. Shearer, S. Chavan, S. Bordiga, S. Svelle, U. Olsbye and K. P. Lillerud, *Chem. Mater.*, 2016, **28**, 3749–3761.